Acta Mech 218, 367–373 (2011)
DOI 10.1007/s00707-010-0420-8

NOTE

F. Zonta · C. Marchioli · A. Soldati

Time behavior of heat fluxes in thermally coupled turbulent dispersed particle flows

Received: 13 March 2010 / Revised: 10 September 2010 / Published online: 30 December 2010

Abstract The effect on heat transfer produced by injection of solid microparticles with high thermal capacity in turbulent channel flow is analyzed. Convection is forced by letting the fluid flow between a hot plate and a cold plate under zero-gravity conditions. An Eulerian–Lagrangian approach based on direct numerical simulation of turbulence (shear Reynolds number $Re^* = 150$ and molecular Prandtl number $Pr = 3$) and on point-particle tracking is used. Full momentum and energy coupling between fluid and particles is considered. Different particle sizes and different particle concentrations are examined.

1 Introduction

Convective transport of heat between a carrier phase (fluid) and a dispersed phase (chemical species, light tracers, heavy particles or droplets) in turbulent dispersed flow is a key feature of many technological and environmental applications. In a previous paper, [1] we put the basis for a sound investigation into turbulent heat transfer phenomena in the case of shear flows where (1) inhomogeneities and anisotropy come into play due to the presence of solid boundaries, mimicking the confinement of the flow in a channel or in a pipe, and (2) heat transfer modifications induced by the presence of a dispersed phase with high heat capacity are explicitely accounted for. Specifically, we characterized the ability of micrometer size particles to promote or damp the turbulent heat transfer mechanisms, and we drew a link between the heat transfer mechanisms and the mass/momentum transfer mechanisms in the context of the Reynolds transport analogy; thus demonstrating that a numerical methodology based on direct numerical simulation (DNS) and Lagrangian particle tracking (LPT) can be used to investigate this type of physical problem.

In this paper, we complete the analysis by adding a quantitative analysis of the heat fluxes when energy and momentum exchange terms are incorporated in the governing equations of both phases. To this aim, the database of [1] has been extended increasing the simulation times and completed performing new simulations with different conditions for particle size (different particle diameters) and particle loading (different mass fractions).

F. Zonta · C. Marchioli (✉) · A. Soldati
Department of Energy Technology, University of Udine, via delle scienze 208, 33100 Udine, Italy
E-mail: marchioli@uniud.it
Tel.: +39-0432-558005
Fax: +39-0432-558027

A. Soldati
Department of Fluid Mechanics, CISM, Udine, Italy
E-mail: soldati@uniud.it

2 Problem formulation and numerical methodology

In this study, a DNS of fully developed particle-laden channel flow with heat transfer is performed. Governing equations and numerical methodology are briefly reviewed to make the paper self-contained: a comprehensive description can be found in [1]. The dimensionless balance equations for the fluid, assumed incompressible and Newtonian, are:

$$\frac{\partial u_i}{\partial t} = -u_j \frac{\partial u_i}{\partial x_j} + \frac{1}{Re^*} \frac{\partial^2 u_i}{\partial {x_j}^2} - \frac{\partial p}{\partial x_i} + \delta_{1,i} + f_{2w}, \quad \frac{\partial T}{\partial t} + u_j \frac{\partial T}{\partial x_j} = \frac{1}{Re^* Pr} \frac{\partial^2 T}{\partial x_j^2} + q_{2w}, \tag{1}$$

where u_i is the ith component of the velocity vector, p is the fluctuating kinematic pressure, $\delta_{1,i}$ is the mean pressure gradient that drives the flow, T is the temperature, Re^* is the shear (or friction) Reynolds number, Pr is the Prandtl number and f_{2w} and q_{2w} are the momentum-coupling and energy-coupling terms, respectively [2]. The shear Reynolds number is defined as $Re^* = u^* h/\nu$, where u^* is the shear velocity,[1] h is the half channel height, and ν is the fluid kinematic viscosity. The Prandtl number is defined as $Pr = \mu c_p/k$ where μ, c_p, and k are the dynamic viscosity, the specific heat, and the thermal conductivity of the fluid, respectively. All variables considered in this study are reported in dimensionless form and expressed in wall units. Wall units are obtained combining u^*, ν and the shear (or friction) temperature $T^* = q_w/\rho c_p u^*$, where $q_w = k \cdot \frac{\partial \overline{T}}{\partial z}|_w$ is the mean heat flux at the wall.

The particle dynamics is described by a set of ordinary differential equations for position ($\mathbf{x_p}$), velocity ($\mathbf{u}_p = \mathrm{d}\mathbf{x}_p/\mathrm{d}t$), and temperature ($T_p$):

$$\frac{d\mathbf{u_p}}{dt} = \frac{\mathbf{u} - \mathbf{u_p}}{\tau_p} \left(1 + 0.15 Re_p^{0.687}\right), \quad \frac{dT_p}{dt} = \frac{(T_f - T_p)}{\tau_T} \left(1 + 0.3 {Re_p}^{\frac{1}{2}} Pr^{\frac{1}{3}}\right), \tag{2}$$

where $\mathbf{u}$ is the velocity of the fluid at particle position, $Re_p = d_p \left|\mathbf{u} - \mathbf{u_p}\right| / \nu$ is the particle Reynolds number, T_f is the temperature of the fluid at particle position, while $\tau_p = \rho_p {d_p}^2/18\mu$ and $\tau_T = c_p \rho_p {d_p}^2/12k$ are, respectively, the particle-velocity and the particle-thermal response times. Here, ρ_p and d_p are particle density and particle diameter, respectively.

The governing equations for the fluid were solved using a pseudo-spectral method based on Fourier–Chebyshev transform of field variables into wavenumber space. Time advancement of the equations is performed using an explicit two-stage Euler/Adams-Bashforth scheme for convective terms and an implicit Crank–Nicolson method for the viscous terms. The reference geometry consists of two infinite flat parallel walls; the origin of the coordinate system is located at the center of the channel and the x-, y-, and z-axes point in the streamwise, spanwise, and wall-normal directions, respectively. Calculations were made at $Re^* = 150$ and $Pr = 3$, with non-dimensional time step size $dt^+ = 0.045$. The size of the computational domain in x, y, and z is $4\pi h \times 2\pi h \times 2h$, corresponding to $1885 \times 942 \times 300$ in wall units. The domain was discretized using an Eulerian grid made of $128 \times 128 \times 129$ nodes. Grid spacing is uniform in the homogeneous x and y directions, and not uniform in z with minimum spatial resolution equal to $\Delta z^+ = 0.0452$ near the wall.[2] Our grid ensures grid-independence statistics, and further grid refinement would not produce quantitative changes in the results (see [1] for further details). Periodic boundary conditions are imposed on both velocity and temperature in x and y; at the wall, no-slip is enforced for the momentum equation whereas constant temperature is assumed for the energy equation. The governing equations for the particles were solved using a Lagrangian tracking routine based on sixth-order Lagrangian polynomials to interpolate velocity and temperature of the fluid at particle location. A fourth-order Runge–Kutta scheme is used for time advancement: the time step size is equal to that used for the fluid and the total tracking time is $t^+ \simeq 4500$. Rigid, spherical particles with density $\rho_p = 19.3 \times 10^3\,\mathrm{kg\,m^{-3}}$ (gold in water) are injected into the flow at average mass fraction, Φ_m, high enough to have significant feedback on both momentum and energy equations (two-way coupling), but negligible particle–particle interactions—see Table 1. The number of individual particles considered is of order $\mathcal{O}(10^5)$ at least. To reduce the otherwise prohibitive computational cost of tracking this many particles, for instance in fully resolved simulations [3], we use the pointwise particle approach. This approach is customary when large particle samples are tracked [4]. Effects due to changes in the specific heats of the fluid on heat transfer are also neglected [5]. Periodic boundary conditions are imposed on particles moving outside the computational

[1] The shear velocity is defined as $u^* = \sqrt{\tau_w/\rho}$, where τ_w is the mean shear stress at the wall and ρ is the fluid density ($\rho = 10^3\,\mathrm{kg\,m^{-3}}$ in this study).

[2] The wall-normal grid spacing is always smaller than the smallest local flow scale to fulfill the requirements imposed by DNS.

Table 1 Summary of simulations and relevant particle parameters

d_p [μm]	d_p^+	τ_p [μs]	$St = \tau_p^+$	τ_T [μs]	$St_T = \tau_T^+$	Φ_m	N_P	Sim.
4	1.2	17.16	1.56	5.49	0.5	3.28×10^{-3}	10^5	S1
						2.62×10^{-2}	8×10^5	S2
8	2.4	68.62	6.24	21.96	2.0	2.62×10^{-2}	10^5	S3
						2.10×10^{-1}	8×10^5	S4

N_p is the number of particles

domain in the homogeneous directions, whereas perfectly elastic rebound is assumed at the smooth walls: in this case, since particles can exchange heat only with the fluid, no thermal coupling is considered between the particles and the wall.

3 Results and discussion

In this section, the modifications induced by particles on the wall-normal heat flux are investigated upon comparison against an unladen pure fluid case.

The time-dependent total heat flux is defined as

$$q(t) = \underbrace{\rho c_p \overline{w'T'}}_{\text{Turbulent Flux}} - \underbrace{k\frac{\partial \overline{T}}{\partial z}}_{\text{Viscous Flux}}, \tag{3}$$

where w' and T' are the velocity and temperature fluctuations of the fluid, respectively. Overbars indicate space average over the homogeneous directions. The effect of particles on heat transport is analyzed using time measurements of $q(t)$ for each simulation of Table 1: these are shown in Fig. 1 for the 4 μm particles and in Fig. 2 for the 8 μm particles.

Let us focus on Fig. 1a first: in the top-half diagram, the time evolution of the total heat flux, $\langle q(t^+)\rangle$, is compared against the heat flux in the unladen flow case, $\langle q^{un}(t^+)\rangle$. Brackets indicate space average over the entire computational domain. Values for $\langle q(t^+)\rangle$ and $\langle q^{un}(t^+)\rangle$ are normalized to the mean value of $\langle q^{un}(t^+)\rangle$. Profiles differ from each other: significant variations, in both positive and negative signs, are observed over the entire time interval. These variations are likely due to particle inertia and to particle thermal inertia, which have an influence on the macroscale amplitude and phase delay with which fluctuations occur with respect to the unladen flow case. To link the behavior of $\langle q(t^+)\rangle$ to the presence of the particles, in the bottom-half diagram of Fig. 1a, the time evolution of the heat transported by the particles, $\langle q_p(t^+)\rangle$, is shown. This quantity is defined as:

$$\langle q_p(t^+)\rangle = \left\langle w_p'(t^+) \cdot \left[T_p(t^+) - T_f(t^+)\right]\right\rangle, \tag{4}$$

where w_p' is the particle wall-normal velocity. The profile of $\langle q_p(t^+)\rangle$ shown in Fig. 1a is obtained upon averaging over the total number of particles and normalized by their mean value. The correlation between $\langle q(t^+)\rangle$ and $\langle q_p(t^+)\rangle$ is qualitatively clear and can be appreciated better in the close-up view of Fig. 1b, which focuses on the time window between $t^+ \simeq 1000$ and $t^+ \simeq 2000$. Local maxima/minima of removable heat flux correspond to values of $\langle q_p(t^+)\rangle$ larger/smaller than the mean, occurring when particles have high positive/negative wall-normal velocity *and* large positive/negative temperature difference with respect to the surrounding fluid. From a physical viewpoint, this suggests that particles can promote or damp the instantaneous thermal fluxes only when, on average, they move quickly to or away from the wall and, at the same time, quickly reach flow regions where they are much hotter or colder than the fluid. The same qualitative observation can be made when different particle concentrations (e.g. $\Phi_m = 2.62 \times 10^{-2}$, simulation S2, Fig. 1c, d) or different particle sizes (e.g. $d_p = 8\ \mu m$, simulations S3 and S4, Fig. 2) are analyzed.

A quantitative evaluation of the physical correlation between the total heat flux $\langle q(t^+)\rangle$ and the heat flux transported by the particles $\langle q_p(t^+)\rangle$ can be obtained by computing their normalized cross-correlation as:

$$r(\tau^+) = \int_{-\infty}^{+\infty} \frac{\langle q(t^+)\rangle \cdot \langle q_p(t^+ + \tau^+)\rangle}{\sigma_q \cdot \sigma_{q_p}} dt^+, \tag{5}$$

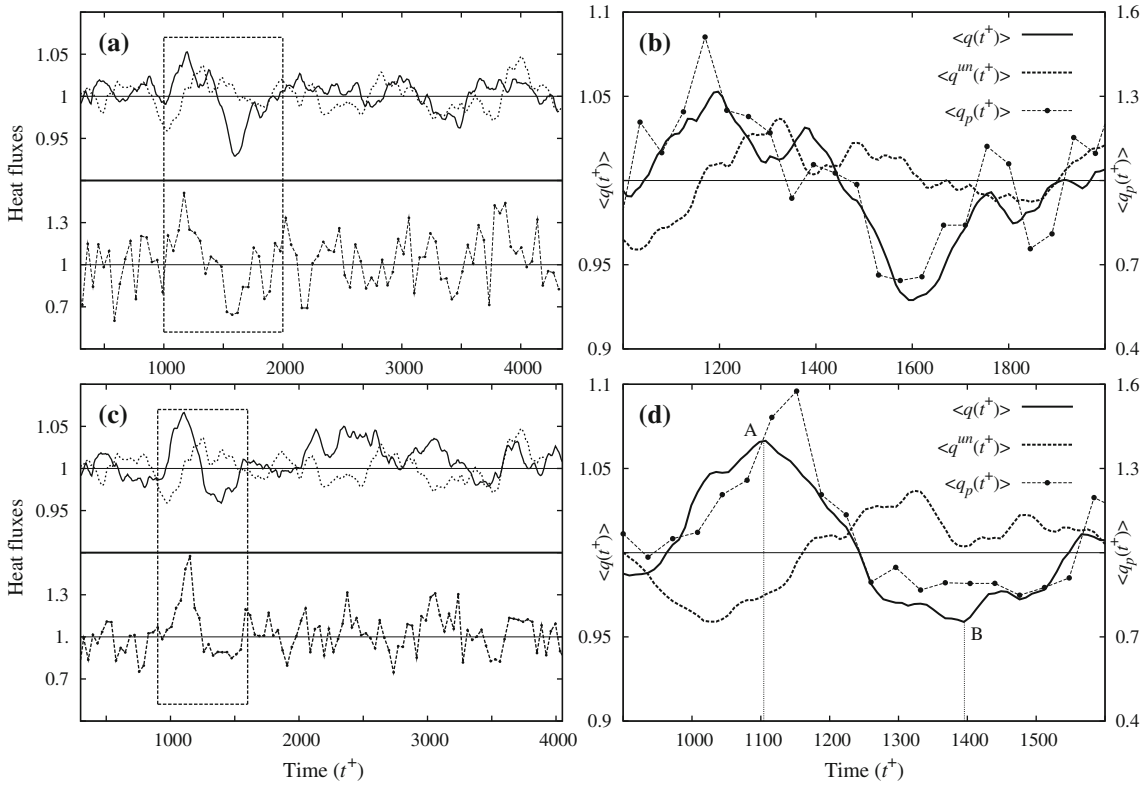

Fig. 1 Time evolution of total heat fluxes for simulations with the 4 μm particles. **a**, **b** Simulation S1 ($\Phi_m = 3.28 \times 10^{-3}$); **c**, **d** simulation S2 ($\Phi_m = 2.62 \times 10^{-2}$). Lines and symbols are as follows: *solid line* total heat flux of the fluid, $\langle q(t^+)\rangle$; *filled circle* heat transported by the particles, $\langle q_p(t^+)\rangle$; *dashed line* total heat flux of the fluid in the unladen flow case, $\langle q^{un}(t^+)\rangle$ (shown for comparison purposes). In the right-hand panels, two different vertical scales (one for $\langle q(t^+)\rangle$ on the left-hand vertical axis, and one for $\langle q_p(t^+)\rangle$ on the right-hand vertical axis) are used to include both profiles in the same diagram

where σ_q and σ_{q_p} represent the standard deviation of the two signals, and τ^+ is the dimensionless time lag between the signals. Figure 3 demonstrates that, in all cases considered, $r(\tau^+)$ exhibits a peak value at $\tau^+ = 0$, indicating that the signals are indeed well correlated. We also performed a Fourier transform of the time series shown for $\langle q(t^+)\rangle$ in Figs. 1 and 2. The aim was to verify the existence of a characteristic frequency f with which the observed large variations in the instantaneous heat fluxes around their time-averaged mean value occur. The resulting transforms $Q(f)$, smoothed by a simple Hann filter, are shown in Fig. 4. All profiles exhibit a peak at $f \simeq 400\,\mathrm{Hz}$ corresponding to a dimensionless Strouhal number $St = f \cdot T_L = 0.664$, where $T_L \sim h/u_\tau \simeq 1.66 \times 10^{-3}$ s represents an estimate of the eddy-turnover time of the large-scale structures in the flow. This frequency is of the order of $1/T_L = 600\,\mathrm{Hz}$ and two orders of magnitude lower than the response frequencies of the particles, which scale with $1/\tau_p$ for the momentum field and with $1/\tau_T$ for the thermal field. This suggests that particle inertia and thermal inertia have a negligible effect on the time scale of thermal fluctuations, which appears to be controlled by the fluid vortices and by the Reynolds transport events that they generate. The ability of the particles to act as effective heat transfer agents is thus intimately connected to the occurrence of strongly coherent motions of a large majority of particles within the turbulent flow. As is well known from several previous papers (see for instance [6] and references therein for more details), these motions are associated with fluxes of streamwise fluid momentum called sweeps, if directed toward the wall, and ejections, if directed away from the wall. From a quantitative viewpoint, the intensity of sweeps and ejections can be characterized using the instantaneous $-\overline{u'w'}$ component of the fluid Reynolds stress tensor. To explore further the connection between heat flux fluctuations and coherent particle motions in Fig. 5a we show the wall-normal profile of $-\overline{u'w'}$ at two specific time instants: $t^+ \simeq 1100$, corresponding to point A in Fig. 1d, which marks the occurrence of a local maximum of $\langle q(t^+)\rangle$, and $t^+ \simeq 1400$, corresponding to point B in Fig. 1d, which marks the occurrence of a local minimum of $\langle q(t^+)\rangle$. The Reynolds stress profile for the unladen flow case (solid line) is also shown for comparison purposes. The heat flux appears enhanced

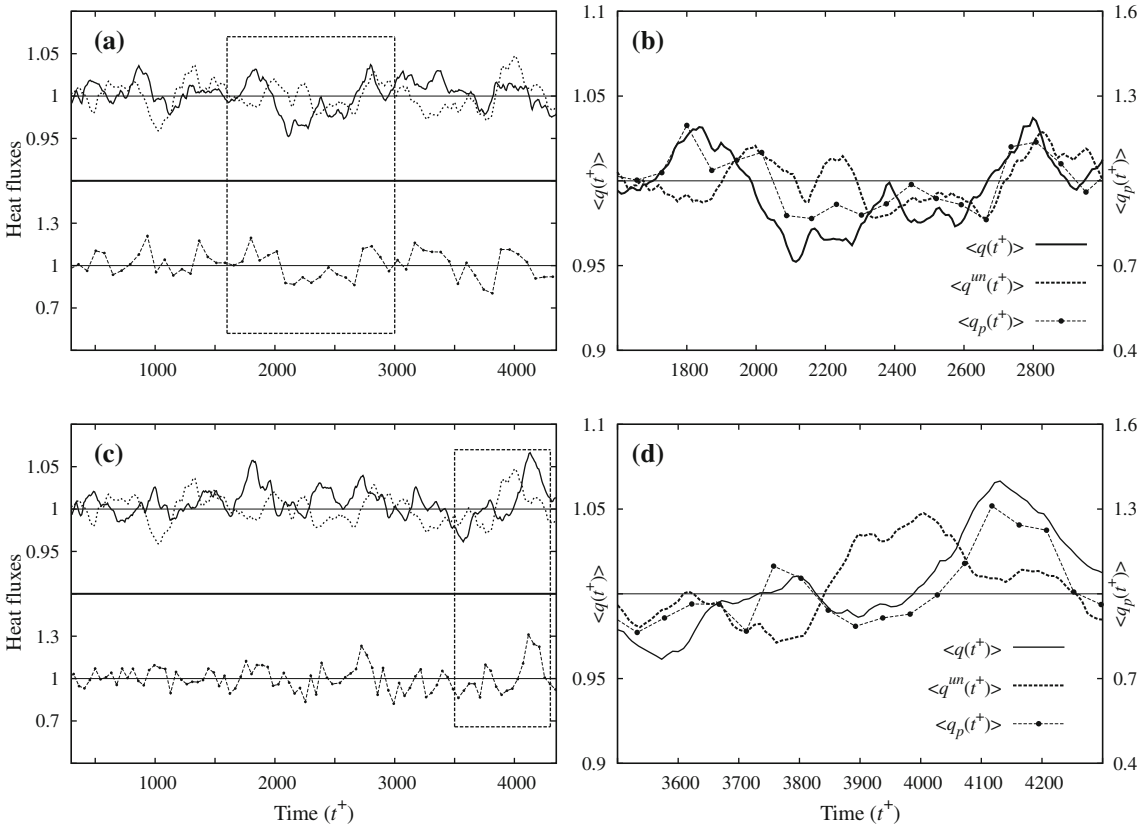

Fig. 2 Time evolution of total heat fluxes for simulations with the 8 μm particles. **a**, **b** Simulation S3 ($\Phi_m = 2.62 \times 10^{-2}$); **c**, **d** simulation S4 ($\Phi_m = 2.1 \times 10^{-1}$). Lines and symbols are as in Fig. 1

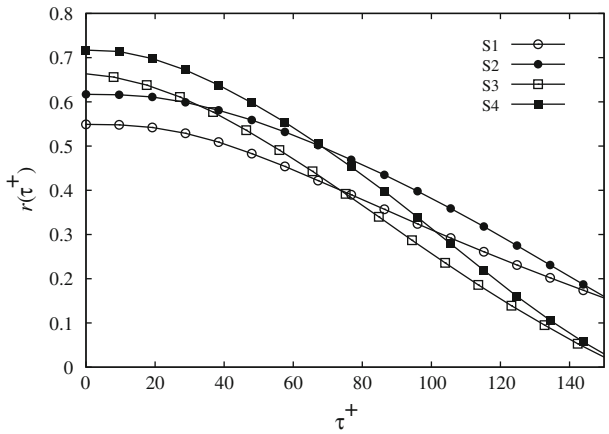

Fig. 3 Cross-correlation coefficient $r(\tau^+)$ between the total heat flux, $\langle q(t)\rangle$, and the heat flux transported by the particles, $\langle q_p(t)\rangle$

when the Reynolds stress transport events in the flow with particles are *on average* stronger than in the unladen flow (case *A*): in this case, it can be argued that entrained particles are more likely to acquire high-wall-normal velocity and, due to their small response times, to decorrelate quickly from the thermal field of the fluid, thus generating larger temperature differences. An opposite behavior is expected when the Reynolds stress transport events are weaker (case *B*), so that the total heat flux is reduced. To confirm this observation, we measured the instantaneous heat fluxes along the wall-normal direction at points A and B: the corresponding profiles are shown in Fig. 5b. Total, turbulent and viscous heat fluxes in dimensionless form are considered to highlight

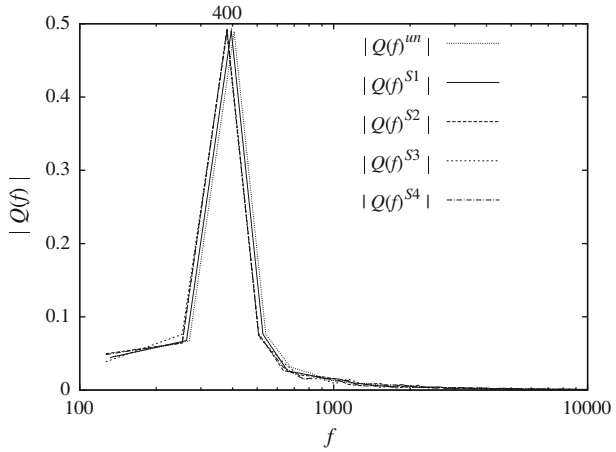

Fig. 4 Fourier transform of $\langle q(t^+)\rangle$ in the frequency space, $|Q(f)|$. $|Q(f)^{un}|$: Fourier transform of $q(t^+)$ in the unladen flow case; $|Q(f)^{S1}|$: Fourier transform of $q(t^+)$ for simulation S1; $|Q(f)^{S2}|$: Fourier transform of $q(t^+)$ for simulation S2; $|Q(f)^{S3}|$: Fourier transform of $q(t^+)$ for simulation S3; $|Q(f)^{S4}|$: Fourier transform of $q(t^+)$ for simulation S4

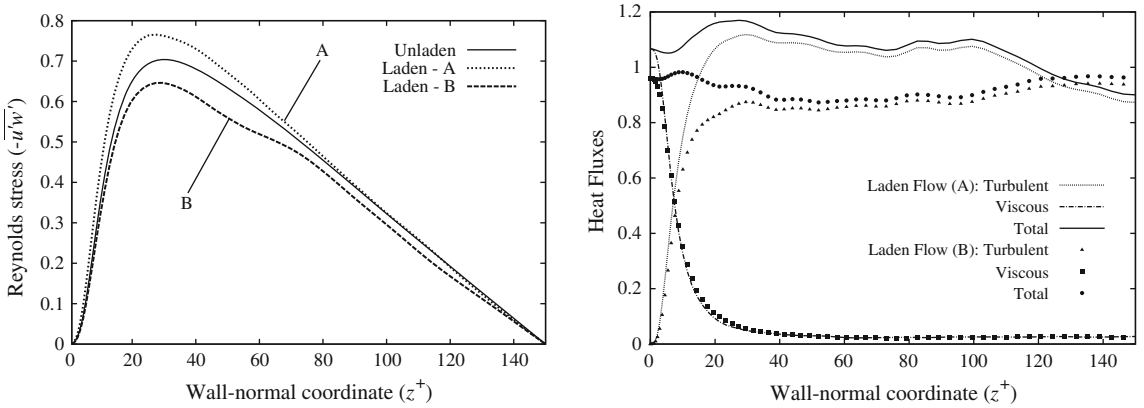

Fig. 5 *Left panel*: instantaneous fluid Reynolds stress ($-\overline{u'w'}$ component): *solid line* unladen flow case; *dotted line* laden flow case (simulation S2) at time $t^+ \simeq 1100$, corresponding to point A in Fig. 1d; *dashed line* laden flow case (simulation S2) at time $t^+ \simeq 1400$, corresponding to point B in Fig. 1d. *Right panel*: instantaneous fluid heat fluxes (simulation S2): lines refer to point A, symbols refer to point B

the relative effect of particles on each quantity. Profiles are normalized by the value of $q/\rho c_p$ at the wall in the unladen flow case. It can be seen that the instantaneous fluxes are not uniform along the channel section and that the total heat flux measured in A is almost everywhere higher than that measured in B, as expected. Differences outside the viscous sublayer are due to changes in the turbulent heat flux (dotted line for point A and black triangles for point B) produced by the convective transport of temperature by the fluid velocity fluctuations in the wall-normal direction. Viscous heat fluxes (dot-dashed line for point A and black squares for point B), which are proportional to the mean wall-normal temperature gradient, nearly coincide in this region and differ only in the vicinity of the wall, where the heat flux measured in A is higher. This result confirms that particles affect heat transport through modifications of the turbulent heat flux almost everywhere in the flow but a thin near-wall region. In this region, convection is no longer effective due to the quick decrease in velocity fluctuations and to the tendency of individual particles to reach local thermodynamic equilibrium with the fluid (thermalization): the main heat transport mechanism is thus diffusion and modifications in the total heat flux are associated with changes in the mean fluid temperature gradient. The situation just described is of general validity and has been observed in all other cases investigated, as we verified examining many uncorrelated flow field realizations for each simulation (results not shown for brevity). Hence, it is fully representative of the influence of particles on the heat transport mechanisms: due to the exchange of momentum and heat between the two phases, the addition of particles modifies quantitatively the transport mechanisms within the fluid, which in turn modify the dynamic (w_p') and thermal (T_p) behavior of the particles.

4 Conclusions and future work

In this paper, we have performed direct numerical simulations of particle-laden liquid-solid turbulent channel flow with heat transfer to investigate the changes in the heat flux of the fluid in the presence of a full (momentum and thermal) two-way coupling between the carrier phase (water) and the dispersed phase (heavy-metal, high-heat-capacity microparticles). Heat transfer modulation induced by particles of different size and concentration is investigated through a quantitative analysis of the time-dependent heat fluxes. Even if the average heat fluxes do not change significantly within the range of parameters investigated in this study, their instantaneous fluctuations change with respect to an unladen pure fluid case. This is due to a different intensity of the instantaneous fluid Reynolds stresses, which can be attributed to the presence of the particles. Acting efficiently on the Reynolds stress events responsible for turbulent transport mechanisms, particles can thus promote or damp the heat transfer process.

From a phenomenological viewpoint, results shown in this paper are of interest in the limit of negligible temperature dependence of the physical properties of the fluid, in particular viscosity. Such coupling can be safely neglected only for small temperature differences; yet this may not always be the case in our problem. From a methodological viewpoint, it would be interesting to test the effect of different boundary conditions for the temperature. Therefore, future developments of this work will be to re-run the simulations presented in this paper with an explicit temperature-dependent relation for the fluid viscosity in the Navier–Stokes equations and with constant heat flux (rather than constant temperature) at the wall.

Acknowledgments Support from PRIN (under Grant 2006098584_004) is gratefully acknowledged.

References

1. Zonta, F., Marchioli, C., Soldati, A.: Direct numerical simulation of turbulent heat transfer modulation in micro-dispersed channel flow. Acta Mech. **195**, 305–326 (2008)
2. Sundaram, S., Collins, L.R.: A numerical study of the modulation of isotropic turbulence by suspended particles. J. Fluid Mech. **379**, 105–143 (1999)
3. Lu, J., Tryggvason, G.: Effect of bubble size in turbulent bubbly downflow in a vertical channel. Chem. Eng. Sci. **62**, 3008–3018 (2007)
4. Nasr, H., Ahmadi, G., Mclaughlin, J.B.: A DNS study of effects of particle–particle collisions and two-way coupling on particle deposition and phasic fluctuations. J. Fluid Mech. **640**, 507–536 (2009)
5. Shotorban, B., Mashayek, F., Pandya, R.V.R.: Temperature statistics in particle-laden turbulent homogeneous shear flow. Int. J. Multiphase Flow **29**, 1333–1353 (2003)
6. Marchioli, C., Soldati, A.: Mechanisms for particle transfer and segregation in turbulent boundary layer. J. Fluid Mech. **468**, 283–315 (2002)